Tomas Bata University in Zlín
Library

Recovery of hydrochloric acid and critical raw materials from an effluent of the copper electrorefining process using electromembrane reactors

Citation

HERNÁNDEZ-PÉREZ, Lorena, María Teresa MONTAÑÉS, Barbora TOMÁŠKOVÁ, Valentín PÉREZ-HERRANZ, and Manuel César MARTÍ-CALATAYUD. Recovery of hydrochloric acid and critical raw materials from an effluent of the copper electrorefining process using electromembrane reactors. *Separation and Purification Technology* [online]. vol. 364, iss. Part 3, Elsevier, 2025, [cit. 2025-09-29]. ISSN 1383-5866. Available at https://www.sciencedirect.com/science/article/pii/S1383586625011839

DOI

https://doi.org/10.1016/j.seppur.2025.132586

Permanent link

https://publikace.k.utb.cz/handle/10563/1012397

This document is the Accepted Manuscipt version of the article that can be shared via institutional repository.

TBU Publications
Repository of TBU Publications
publikace.k.utb.cz

Recovery of hydrochloric acid and critical raw materials from an effluent of the copper electrorefining process using electromembrane reactors

L. Hernández-Pérez[a], M.T. Montañés[a], B. Tomášková[b], V. Párez-Herranz[a], M. C. Martí-Calatayud[a,*]

[a]*IEC Group, ISIRYM, Universitat Politècnica de València, Camí de Vera s/n, 46022, València, P.O. Box 22012, E-46071, Spain*

[b]*Department of Environmental Protection Engineering, Tomas Bata University in Zlin, Faculty of Technology, Vavreckova 275, 760 01 Zlin, Czech Republic*

[*]*Corresponding author. E-mail address: mcmarti@iqn.upv.es (M.C. Martí-Calatayud).*

ABSTRACT

Highly concentrated acids are used to regenerate ion-exchange resins that are applied for the removal of metallic impurities (i.e. antimony, arsenic and bismuth) from spent copper electrorefining baths, thus generating acidic effluents. In this work, the recovery of critical raw materials and HCl from a real effluent is evaluated by electrodeposition using reactors with and without membrane separators. First, four reduction peaks were detected by cyclic voltammetry, and their correspondence to the pairs Cu(II)/Cu(I), As(III)/As, Sb(III)/Sb, Bi(III)/Bi, and Cu (I)/Cu was confirmed by potentiostatic electrodeposition and elemental analysis of the deposits. A high selectivity towards antimony deposition over arsenic and copper was achieved at the least cathodic applied potential (—0.25 $V_{Ag/AgCl}$), obtaining a deposit with 85 wt% of antimony and bismuth as the second most deposited metal. At more cathodic potentials, deposition of copper takes place and the antimony content in the deposits decreases.

Galvanostatic electrodeposition tests were carried out using a three-compartment reactor. Results showed that the transport rate of Cl^- ions through the anion-exchange membrane is too slow to recover highly concentrated HCl in a separate compartment. However, electrodeposition of the main elements present in the real effluent makes possible obtaining impurity-free HCl (4.8 M) in the cathodic compartment. The complete recovery of antimony (100 %) and almost complete recovery of bismuth (95 %) and copper (90 %) were achieved after 4 h working at —100 mA·cm^{-2}. Tests conducted with a single-compartment reactor confirmed that formation of chlorine gas at the anode causes the redissolution of the metals deposited at the cathode, thus revealing that electromembrane reactors improve the electrodeposition current efficiency.

Keywords: Acidic effluents, antimony, metal recovery, electrodeposition, cyclic voltammetry, critical raw materials, electromembrane reactors

1. Introduction

The EU issues periodically a list of critical raw materials, based on their economic importance and high supply risk [**1**]. In the same line, a list of critical minerals has also been released by the U.S. Geological Survey [**2,3**]. Both lists include antimony, bismuth and arsenic and highlight the need to obtain these materials from secondary sources, either by recycling products at the end of their useful life or by recovering them from waste. Antimony is mainly used in alloys to increase the hardness and resistance towards oxidation of other metals, which are used in lead-acid batteries, ammunition, bearings, or diodes, among other applications [**4**]. In addition, antimony trioxide is used as flame retardant, and as catalyst in the production of polyethylene tere-phthalate [**5,6**]. Bismuth is used in multiple fields such as cosmetics, the pharmaceutical industry, or in metallurgical applications [**7**]; and arsenic is used in aeronautics, fuel cells and digital technologies [**8**].

The extraction of copper from ores and its subsequent electrorefining is one of the industrial processes where the presence of antimony, bismuth and arsenic as secondary materials is most notable [**9,10**]. The production of copper is carried out through two different processes: hydrometallurgy, which is used with copper oxides and mixed minerals, and pyrometallurgy, which is used with copper sulfide ores [**10**]. In the pyrometallurgical process, the minerals are first processed by grinding and crushing, and then a copper concentrate is obtained after subsequent flotation, filtration and drying stages [**11**]. This copper concentrate is transformed by smelting, producing copper plates with a purity of 99.5 %, which are used as anodes in an electrorefining process to obtain copper cathodes of higher purity, 99.99 % [**12**]. During the electrorefining, the impurities of antimony, bismuth and arsenic contained in the anode dissolve together with copper because the standard reduction potentials of the four elements are similar [**13**]. The buildup of impurities in the electrolyte generates several problems, as they affect the quality of the final product [**14**] and passivate the anodes [**15**]. The impurities are commonly removed from the electrolyte using selective ion-exchange resins, thus allowing the reuse of sulfuric acid and copper in the electrorefining process [**16,17**]. When the ion-exchange capacity of the resins is reached, they are regenerated using highly concentrated hydrochloric acid (up to 6 M HCl), which results in a strongly acidic residual effluent that contains the metals that were previously retained in the resins, mainly antimony.

The effluent resulting from the regeneration of ion-exchange resins in copper metallurgy has been traditionally treated by distillation to recover part of the acid in the distillate stream [**18**]. A waste liquor containing the extracted metal impurities is obtained as by-product, which is precipitated by adding gypsum, and the resulting sludge is deposited in landfills [**19**]. Another common treatment is the neutralization of the effluent with lime. In this way, the resulting product can be eliminated as a toxic waste [**20**] or recovered as a metal oxide that is used as raw material to produce antimony-based flame retardants [**21**] or electrical quality bismuth [**22**]. Currently, other processes have been developed to recover antimony and bismuth from the resin eluates, such as liquid-liquid extraction [**20**] or selective precipitation by adding sodium hydroxide and ammonium hydroxide [**23**]. Given that the pH level of the waste effluent can reach even negative values, most of the mentioned techniques require the addition of large amounts of chemicals for neutralization, limiting the continuous reuse of hydrochloric acid as a resin regenerating agent and even assuming the loss of antimony and bismuth. Compared to the techniques that are currently used, electrochemical processes represent a more environmentally friendly alternative to treat the effluent under study.

Electrochemical techniques offer multiple advantages: they do not require the addition of reagents [**24**] and can ensure a high efficiency and selectivity through an adequate control of operating parameters [**25-27**]. They have gained relevance in the recovery of strategic metals from wastewaters because they can work at room temperature, are easily applied at industrial scale [**28**], and can be

powered by renewable energy sources [**29**]. Among the different electrochemical techniques for the recovery of strategic metals present in industrial and mining effluents, electrodeposition stands out because the metals can be directly separated in solid form at the cathode [**30-32**].

In our previous studies, electrodeposition of antimony from highly concentrated synthetic HCl solutions was investigated [**33,34**]. One of the main challenges identified when this process is conducted with highly acidic electrolytes is the competition between the reduction of metals at the cathode and the Hydrogen Evolution Reaction (HER), which decreases the electrodeposition rates and affects the structure of the metal deposits [**33**]. Besides this, the products of anodic reactions can also alter the processes taking place at the cathode, because they can participate in cathodic reactions, or even react with the deposited metals [**34**]. Research on metal recovery from multicomponent mixtures containing antimony, bismuth and arsenic has been conducted in previous works [**35-37**]. In the specific case of mixtures including antimony and bismuth, it was observed that the applied current density and the anti-mony/bismuth electrolyte concentration play a role on the selectivity and electrodeposition efficiency of both metals [**38**]. All previous works reveal that control on the electrochemical operating conditions, as well as on the interactions between the different electrochemical reactions taking place at both electrodes determine the process efficiency.

In this work, electrodeposition is further investigated using electromembrane reactors as a treatment process for a real eluate resulting from the regeneration of ion-exchange resins in the copper industry. The objective of the process is to recover the metals present in this acidic effluent, which in turn will allow reusing the hydrochloric acid for the regeneration of the resins. In this way, progress will be made towards full circularity and sustainability of copper electrorefining; as well as towards process cost reduction, since the purchase of acid as primary raw material is one of the main operating costs [**18**]. Voltammetric tests have been conducted to characterize the electrochemical behavior of the real effluent and, subsequently, the morphology and composition of the deposits formed during short-term electrodepositions at different cathodic potentials have been examined. Long-term electrodepositions have been conducted in galvanostatic mode, where the applied current and the use of membranes have been investigated in order to minimize the HER reaction and separate the events taking place at the cathode and the anode.

2. Material and methods

2.1. Characteristics of the effluent

The solution under investigation is the real effluent produced during the regeneration of the ion-exchange resins used to remove impurities from the copper electrorefining electrolyte, which has been supplied by the company Atlantic Copper, S.L.U., located in Spain. The composition of the effluent was determined using Inductively Coupled Plasma Mass Spectrometry (Thermo Scientific iCAP RQ ICP-MS) and is shown in **Table 1**. The major impurity is antimony followed by arsenic, copper and bismuth. It also contains other impurities (i.e. Fe, Pb, Ni, Zn and Cd), but their concentration has been considered negligible for the present study. In our previous studies [**33,34,38**], we worked with synthetic solutions based on the effluents from Chilean metallurgical facilities. The composition shown in **Table 1** is consistent with that observed in Chilean effluents, where antimony is also the main impurity detected in the el-uates resulting from the regeneration of ion-exchange resins [**16,39**]; furthermore, the rest of the metals are the same, although they are present in different concentrations.

The concentration of hydrochloric acid (HCl) in the solution is 5.6 M and was determined by means of the Mohr's method. This method consists of titrating with silver nitrate ($AgNO_3$) using potassium chromate (K_2CrO_4) as an indicator. This concentration is consistent with the range reported in literature for the regeneration of ion-exchange resins, which varies between 4 and 6.7 M, and corresponds to extremely low pH values between — 1 and 0 [**16**].

2.2. Cyclic and linear voltammetric tests

The electrochemical characterization of the effluent has been carried out at room temperature using two different electrochemical cells, both with a volume capacity of 50 mL, a three-electrode configuration and a potentiostat/galvanostat (Autolab PGSTAT 302). Cyclic voltammetric measurements were conducted under static conditions in an in-house designed cell with the working electrode in a face-up position in order to facilitate the release of gas bubbles generated during the tests; the working electrode was a platinum electrode (Metrohm for Autolab RDE) with an effective area of 0.071 cm^2. Linear sweep voltammetry was performed in a conventional cell under hydrodynamic conditions with a rotating disk electrode (RDE, Autolab RDE-2 Metrohm) at a rotational speed of 500 rpm; the working electrode was a copper bar with an effective area of 0.8 cm^2. In both cyclic and linear sweep voltammetry, the reference electrode was a standard Ag/AgCl (3 M KCl) electrode; the counter electrode was a platinum ring with an area of 1 cm^2 (Mettler-Toledo); and the scan rate was 10 $mV{\cdot}s^{-1}$. In the cyclic voltammetric tests the scans started at the open circuit potential (OCP) in the direction towards more cathodic potentials; and several cycles were carried out to ensure stabilization of the system. In the linear sweep voltammetry, only the cathodic polarization curve was obtained.

Before performing each test, the working electrodes were polished with 500 and 4500 grit sandpaper; then, they were rinsed with distilled water and ethanol, and dried with air.

Table 1 Composition of the effluent determined by ICP-MS.

Element	Sb	As	Cu	Bi	Fe	Pb	Ni	Zn	Cd
Concentration (mM)	188.81	40.20	16.46	12.61	0.41	0.29	0.16	0.11	0.07

2.3. Short-term electrodepositions

Short-term electrodeposition tests (30 min) were carried out in potentiostatic mode at room temperature. The cell and electrodes are the ones used for the linear sweep voltammetry. Electrodepositions were performed with a rotational speed of 500 rpm at three electrode potentials selected from the linear voltammograms: —0.25, —0.40 and - 0.60 $V_{Ag/AgCl}$.

The main objective of these tests was to analyze the morphology and composition of the formed deposits to correlate the reduction peaks observed in the voltammetric study with their corresponding reactions. For this purpose, field emission scanning electron microscopy ($FESEM$) and energy dispersive X-ray spectroscopy (EDX) were used. A ZEISS Ultra 55 microscope was employed, which has an energy dispersive X-ray detector (EDX, Oxford Instruments) attached. An acceleration voltage of 10 kV was applied.

2.4. Long-term electrodepositions

Long-term electrodepositions (4 h) were conducted in galvanostatic mode at room temperature. A rectangular (5.9 x 3.4 cm) sheet of copper with an effective area of 20 cm^2 was used as the cathode. A dimensionally stable anode (DSA) composed of titanium coated with a mixed metal oxide (RuO_2/IrO_2: 0.70/0.30) and an area of 40 cm^2 was used as anode. The reference electrode was a standard Ag/AgCl (3 M KCl) electrode. Electrodepositions were performed at two current densities, —50 and —100 mA/cm^2, which were selected from the linear voltammogram.

Two types of reactors have been used in the long-term electrodepositions, one with a single-compartment with a volume capacity of 250 mL and another reactor with three compartments, with a 250 mL volume capacity each. To work under hydrodynamic conditions, magnetic stirrers with a stirring rate of 500 rpm were used. **Fig. 1** shows a scheme of the three-compartment reactor. An anion-exchange membrane (AMV-N, Selemion) was used to separate the cathodic and central compartments, and a cation-exchange membrane (Nafion 117, Dupont) to separate the central and the anodic compartment. The effluent under investigation was introduced into the cathodic compartment; a 1 M HCl solution in the central compartment, and 0.5 M H_2SO_4 in the anodic one (both prepared using analytical-grade reactants from Panreac). With this configuration, the oxidation of chloride ions in the anodic compartment is prevented, while they can be concentrated in the central compartment via their transport through the anion-exchange membrane.

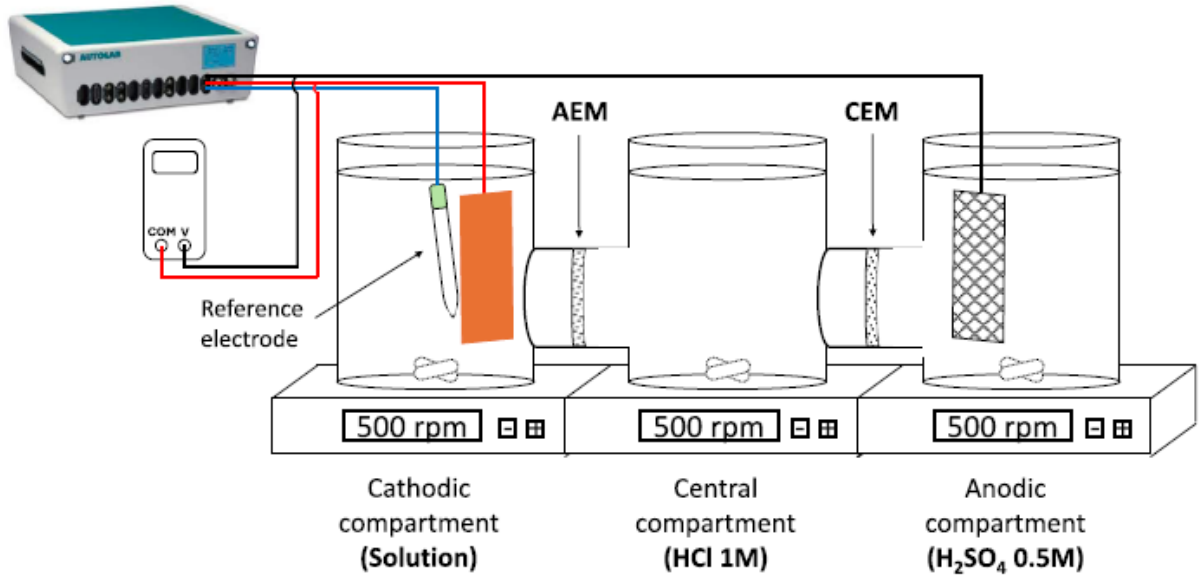

Fig. 1. Schematic diagram of the three-compartment electrochemical reactor. AEM: anion-exchange membrane; CEM: cation-exchange membrane.

During the tests, the evolution of the cathode potential and the cell voltage was recorded. In addition, catholyte samples were taken from the reactor every 30 min. These samples were analyzed by atomic absorption spectroscopy using a Perkin-Elmer (model AAnalyst 100) flame spectrometer. Four hollow cathode lamps supplied by Varian Techtron Pty. Ltd. were used to determine the concentration of antimony, bismuth, arsenic and copper. **Table S1 of the Supplementary material** shows the wavelength, spectral bandwidth and current values used to measure each element. When working with the three-compartment reactor, samples were taken from both the cathodic and the central compartment, to analyze the evolution over time of the chloride concentration by means of the Mohr's method.

3. Results and discussion

3.1. Electrochemical characterization

Fig. 2 shows a cyclic voltammogram registered with the effluent under study. To facilitate the analysis of the electrochemical behavior of the system, a cyclic voltammogram obtained under the same conditions with a synthetic solution of 10 mM Sb, 2.5 mM Bi and 6 M HCl has also been included; this voltammogram was obtained in a previous study where the composition of similar eluates generated in Chilean metallurgical industries were considered [**38**]. The real effluent under study contains more elements than the synthetic solution and, in addition, the concentration of Sb and Bi is higher; however, the voltammogram of the synthetic solution can be helpful for identifying reduction and oxidation reactions observed in the voltammogram of the real effluent.

Starting the analysis of the voltammograms from the OCP value in the cathodic direction, a reduction peak (peak C1) is observed in both systems at very similar potentials: — 0.28 $V_{Ag/AgCl}$ for the synthetic solution, and — 0.34 VAg/AgCl for the real effluent. In the case of the synthetic solution, this peak corresponds to the simultaneous reduction of Sb and Bi according to Eq. (**1**) [**38,40**]; therefore, for the real effluent the peak C1 can also be related to the reduction of these two elements.

$$x\,BiCl_5^{2-} + y\,SbCl_6^{3-} + 3\cdot(x+y)e^- \rightarrow Bi_xSb_y + (5x+6y)\,Cl^- \qquad (1)$$

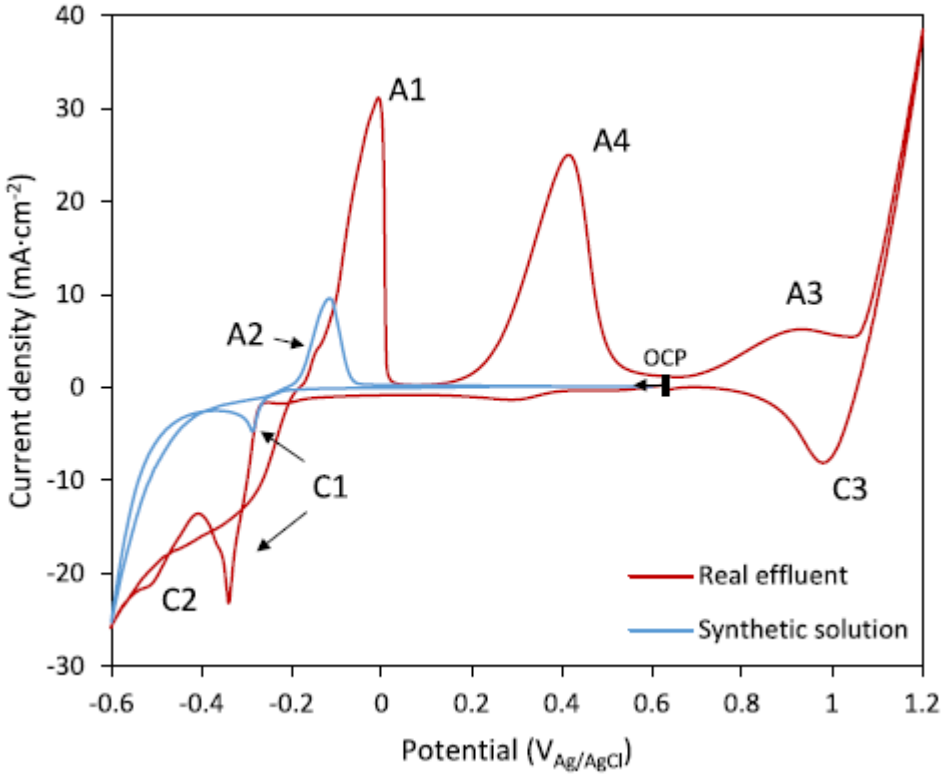

Fig. 2. Comparison between cyclic voltammograms registered for the real effluent under study (red line) and for a synthetic solution containing 10 mM Sb, 2.5 mM Bi and 6 M HCl (blue line).

After peak C1, HER occurs for the synthetic solution, whereas for the real effluent another reduction peak (peak C2) is observed at approximately —0.5$V_{Ag/AgCl}$. Therefore, this peak C2 may be related to the electrodeposition of species other than Sb or Bi. After peak C2, HER also predominates in the real effluent.

Regarding the anodic scan, an oxidation peak (peak A1) beginning at —0.2 $V_{Ag/AgCl}$ is observed in both solutions, which is attributed to the oxidation of the elements that have been previously reduced in the peak C1. With the real effluent, in addition to peak A1, two new peaks are observed: peak A2 that appears as a shoulder of peak A1, and peak A4 at + 0.4 $V_{Ag/AgCl}$. We hypothesize that these two peaks may correspond to the oxidation of the species that are reduced in the peak C2. In addition, at more anodic potentials, peak A3 is observed. When the electrochemical behavior of synthetic antimony solutions in 6 M HCl was studied in depth, the peak that appeared at potentials similar to the peak A3 was attributed to the oxidation of Sb(III) to Sb(V) [**33**]. Following the peak A3, the increase in current density is attributed to the oxidation of chloride ions to chlorine gas. In the synthetic solution, the evolution of chlorine gas was not observed because the voltammogram ends at + 0.6 $V_{Ag/AgCl}$. After reverting the scan from the anodic limit potential towards OCP, peak C3, located near + 1 $V_{Ag/AgCl}$, was identified. This peak could be related to the reduction of Sb(V) to Sb(III) or the reduction of chlorine to chloride ions.

In order to verify the hypotheses raised above about the observed peaks, several cyclic voltammograms with the real effluent have been registered, in which the cathodic inversion potential has been varied taking the following values: —0.3, — 0.4, — 0.6 and - 8 $V_{Ag/AgCl}$ (**Fig. 3**a). When the potential is inverted at - 0.3 $V_{Ag/AgCl}$], the peak A1 is observed because the reduction of the elements has already begun, and the peak A3 is also detected. This confirms that peak A1 corresponds to the reverse reaction occurring at peak C1. If the potential is reversed at - 0.4 $V_{Ag/AgCl}$], the current density of the peak A1 increases considerably because the potential of the peak C1 has already been reached and a larger mass amount of the elements has been deposited. When the potential is inverted at - 0.6 $V_{Ag/AgCl}$, the potential of the peak C2 is exceeded and consequently the peaks A2 and A4 appear, confirming that they correspond to the oxidation of the species that have been reduced previously in the peak C2. If the cathodic inversion potential is extended to - 0.8 $V_{Ag/AgCl}$, no new oxidation peaks appear, only the HER takes place vigorously and the current density of the observed anodic peaks increases.

Fig. 3b shows a magnification of the cathodic branch between — 0.6 and $+ 0.5\ _{V Ag/AgCl}$ of the voltammograms presented in **Fig. 3**a. In this magnification two additional peaks are observed, peak C0 at approximately — 0.2 $V_{Ag/AgCl}$, and peak C4 at + 0.3 $V_{Ag/AgCl}$. Neither of these two peaks is observed for the synthetic solution (**Fig. 2**); therefore, they may be related to the electrodeposition of species other than Sb or Bi. Shu et al. [**41**] detected the reduction peak of As(III) to metallic As at — 0.20 $V_{Ag/AgCl}$, with a solution containing arsenic in hydrochloric acid medium and using a glassy carbon electrode. In that study, antimony solutions were also investigated, and the reduction of Sb(III) to metallic Sb was observed at more cathodic potentials than those for the As reduction, more specifically, at — 0.30 $V_{Ag/AgCl}$. The difference between the reduction potentials of As and Sb in the aforementioned study is similar to that observed between the peaks C1 and C0 in **Fig. 3** (0.14 V); thus, peak $C0$ could be attributed to the reduction of As(III) to metallic As. Since the reduction of arsenic begins at potentials more negative than —0.20 $V_{Ag/AgCl}$, the peak A1, may be associated not only with the oxidation of the Sb and Bi deposited in the peak C1, but also with the oxidation of As to As(III).

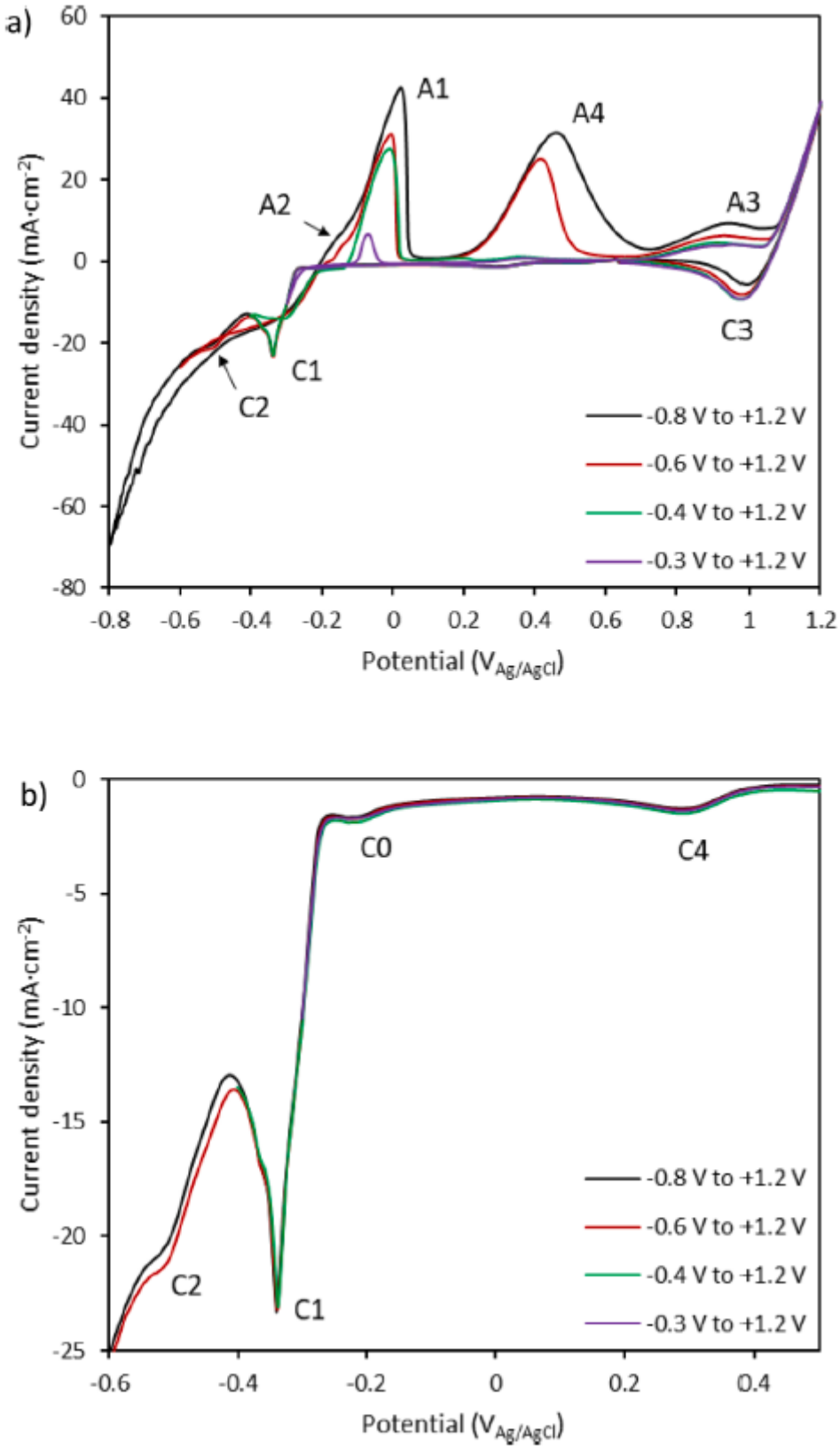

Fig. 3. Cyclic voltammograms registered for the real effluent under study at different cathodic inversion potentials (a). Magnification of the reduction peaks C1 and C2 (b).

The peak C4, along with the peaks C2, A2, and A4, could be related to redox reactions involving copper. Wu et al. [**42**] observed peaks similar to those in **Fig. 3**, with a system containing copper and antimony in a hydrochloric acid medium. These authors detected a peak located at + 0.31 $V_{Ag/AgCl}$ that was attributed to the reduction of Cu(II) to Cu(I); and this potential almost coincides with that of the peak C4 (+ 0.3 $V_{Ag/AgCl}$). They also observed the reduction peak of Sb(III) to metallic Sb at - 0.27 $V_{Ag/AgCl}$, that is a similar potential to that of the peak C1 (—0.28 $V_{Ag/AgCl}$). After the Sb(III)/metallic Sb reduction peak, these authors observed a peak at — 0.34 $V_{Ag/AgCl}$ associated with the reduction of Cu(I) to metallic Cu, which is the same as the peak C2. Regarding the anodic scan, they detected two oxidation peaks and a subpeak located to the left of the oxidation peak of metallic Sb to Sb(III), which began at — 0.06 $V_{Ag/AgCl}$; this subpeak was associated with the oxidation of metallic Cu to Cu (I), and it resembles the subpeak A2. The other oxidation peak, located at + 0.5 $V_{Ag/AgCl}$, was assigned to the oxidation reaction of Cu(I) to Cu (II); which is similar to that of the peak A4 (+ 0.4 $V_{Ag/AgCl}$).

In summary, the voltammetric study allows us to assign the peak C0 to the reduction of As(III) to metallic As. In line with the results obtained in our previous studies with synthetic solutions [**38**], the pair of peaks C1 and A1 correspond to the redox reactions of Sb(III)/metallic Sb and Bi(III)/metallic Bi. The peak C2, together with the subpeak A2, represent the metallic Cu(I)/Cu redox process; and the peaks A4/C4 are related to the oxidation and reduction, respectively, of the Cu(II)/Cu(I) pair. Finally, the peak A3 corresponds to the oxidation of Sb(III) to Sb(V).

After the cyclic voltammetric analysis, a linear sweep voltammetry was performed using the same cell, electrode and hydrodynamic conditions to be used in the short-term electrodepositions. **Fig. 4** shows the registered linear voltammogram, where three reduction waves R0, R1 and R2 are observed, at — 0.25, —0.40 and — 0.60 $V_{Ag/AgCl}$, respectively. These waves can be related to three of the reduction peaks detected in the cyclic voltammograms, specifically to the peaks C0, C1 and C2 (**Fig. 3**). Although the reduction potentials are very close to those obtained in the cyclic voltammograms, it is interesting to note that the values of current density registered with this setup are significantly larger. The larger current densities are a consequence of the improved supply of dissolved electroactive species towards the electrode surface, which is ensured by the convective regime resulting from the rotating speed of 500 rpm. In our previous studies with synthetic solutions [**34**], we proved that the electrodeposition of Sb(III) in highly concentrated hydrochloric acid solutions is a mass transfer-controlled process and it is possible to increase its recovery by improving hydrodynamic conditions.

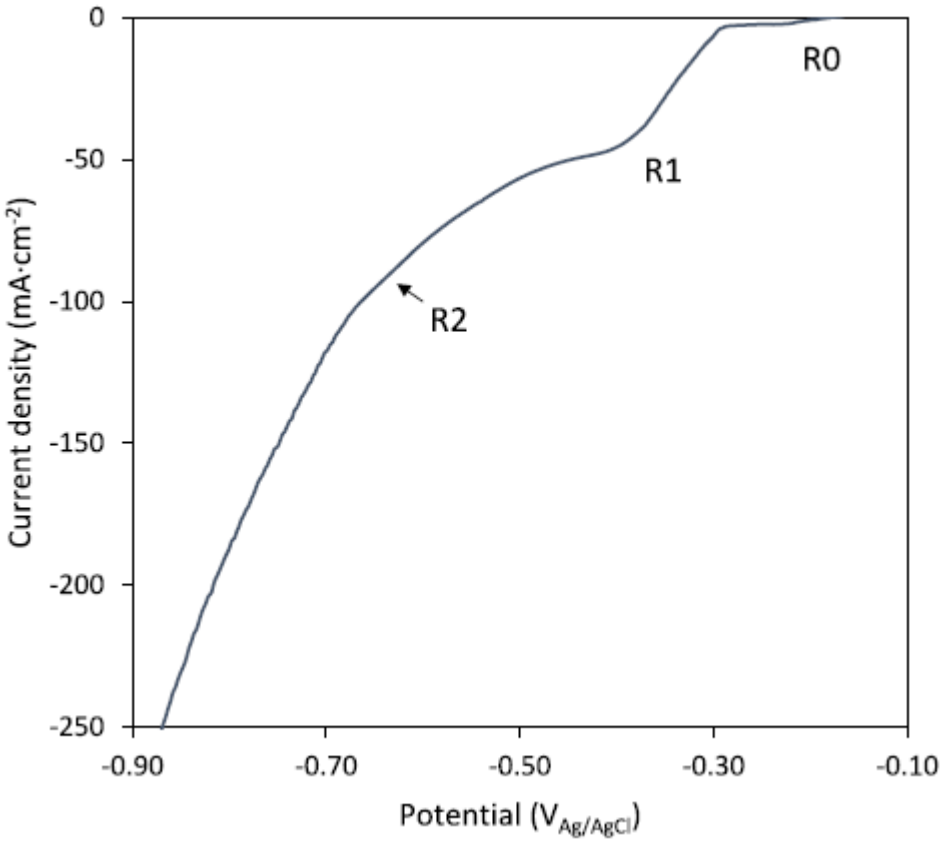

Fig. 4. Linear voltammogram registered for the real effluent under study at 500 rpm.

3.2. Short-term electrodepositions in potentiostatic mode

In order to analyze the deposits obtained with the real effluent, shortterm electrodepositions (30 min) have been carried out, using the conventional three-electrode cell with the RDE and a copper electrode as working electrode. The electrodepositions have been performed in potentiostatic mode at three electrode potentials: —0.25, —0.40 and —0.60 $V_{Ag/AgCl}$, corresponding to the reduction waves R0, R1 and R2 observed in **Fig. 4**.

Fig. 5 shows the SEM images of the deposits obtained at the three applied potentials. The deposits generated at — 0.25 $V_{Ag/AgCl}$ (**Fig. 5**a) and at — 0.40 $V_{Ag/AgCl}$ (**Fig. 5**b) show a uniform granule-shaped structure. In contrast, the deposit obtained at — 0.65 $V_{Ag/AgCl}$ presents a dendritic and non-uniform structure. The predominance of dendritic deposits is typical of systems where the formation of gas products takes place concomitant to the formation of the deposits. These results are consistent with the increasing relevance of the HER when the applied potential is more cathodic. Similar deposits were also obtained under these conditions in our previous study containing only antimony as the dissolved metal [**33**].

The composition of the deposits has been analyzed by means of EDX spectroscopy. **Table S2 of the Supplementary material** and **Fig. 6** show the obtained values, where it can be seen that antimony is the main species electrodeposited for all applied potentials. The amount of antimony in the deposit decreases when more negative potentials are applied; this may be because, at more cathodic potentials, the reduction of the rest of the elements present in the real effluent also occurs. The amount of bismuth reaches its maximum value at the intermediate applied potential (— 0.40

$V_{Ag/AgCl}$). Concerning arsenic, the weight percentage of this species in the deposit increases when more negative potentials are applied; thus, it can be concluded that, despite the fact that the As reduction peak is the least cathodic, its deposition is favored when applying more cathodic conditions. Regarding the rest of the elements present in the effluent, lead is not deposited at any applied potential; cadmium and zinc are deposited at the least cathodic applied potential but are not detected at the other potentials; and iron begins to be deposited at — 0.60 $V_{Ag/AgCl}$. Finally, copper could be detected either because it is the cathode material or because it is deposited from the effluent. Since the weight percentage of copper in the deposit increases when the applied potential becomes more negative, it can be concluded that it is indeed electrodeposited over the cathode. Moreover, the rate of copper deposition increases when the applied potential is more cathodic because the Cu reduction peak is the most cathodic one. In this regard, the trend of the percentage of copper deposited confirms that both the reduction peak C2 (**Fig. 3**) and the wave R2 (**Fig. 4**) correspond to the reduction of Cu(I) to metallic Cu.

Table 2 shows the molar ratio between antimony and the other three major elements (arsenic, copper, and bismuth), both in the initial composition of the real effluent and in the obtained deposits; these ratios have been calculated from data in **Table 1** and **Table S2**, respectively. According to the values in **Table 2**, the electrodeposition process shows a great selectivity towards antimony over arsenic because, at all applied potentials, the molar ratio nSb/nAs in the deposit is much higher than the one corresponding to the real effluent under study. Nonetheless, the selectivity decreases as more negative potentials are applied, which indicates that the least cathodic conditions are also the ones which lead to the highest selectivity towards antimony. The electrodeposition process also shows selectivity towards antimony over copper at the two less cathodic applied potentials because the molar ratio nSb/nCu is higher in the deposit than in the effluent under study; however, at — 0.6 $V_{Ag/AgCl}$, the process becomes rather selective towards copper. These results show good agreement with the results obtained in the voltammetric study, since the reduction of copper occurs at that potential value (see R2 in **Fig. 4**). Finally, the electrodeposition process does not present selectivity towards antimony over bismuth at any of the applied potentials because the molar ratio nSb/nBi is higher in the effluent under study than in the resulting deposits; in addition, the ratio nSb/nBi in the deposits also diminishes as the applied potential becomes more negative.

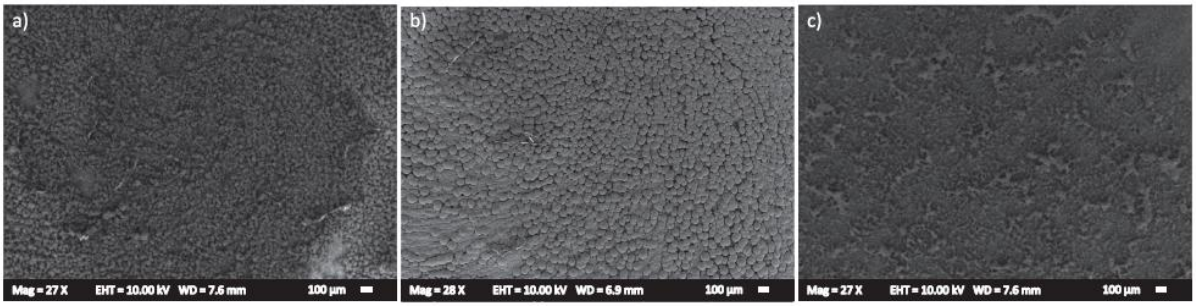

Fig. 5. SEM images of the deposits obtained at different applied potentials: 025 $V_{Ag/AgCl}$ (a); _ 040 $V_{Ag/AgCl}$ (b); and _ 065 $V_{Ag/AgCl}$ (c).

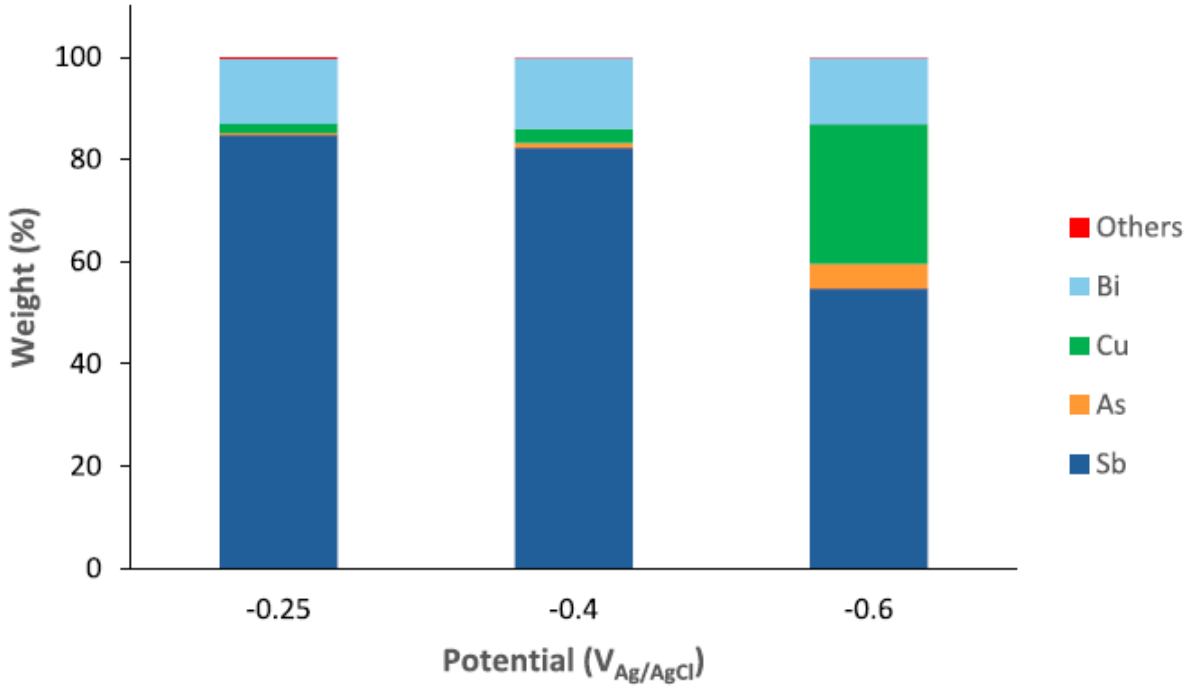

Fig. 6. EDX analysis of the deposits showed in **Fig. 5**.

Table 2 Molar ratio between antimony and the other three major elements (arsenic, copper and bismuth) in the effluent under study and in the deposits obtained at different applied potentials.

Molar ratio	Real effluent under study	Deposit obtained at −0.25 $V_{Ag/AgCl}$	Deposit obtained at −0.40 $V_{Ag/AgCl}$	Deposit obtained at −0.60 $V_{Ag/AgCl}$
n_{Sb}/n_{As}	4.7	172.9	54.5	7.1
n_{Sb}/n_{Cu}	11.5	23.2	15.5	1.0
n_{Sb}/n_{Bi}	15.0	11.5	10.1	7.2

After analyzing the previous results, we can conclude that it would be possible to obtain a deposit with a high content in antimony (85 wt%) working at the least cathodic potential studied, — 0.25 $V_{Ag/AgCl}$.

3.3. Long-term electrodepositions in galvanostatic mode

Long-term electrodepositions (4 h) have been carried out using two different reactor configurations, one consisting of a membrane reactor with three different compartments and the other one with a single compartment, both described in section 2.4. The objective of these electrodepositions is to extract the elements in the form of a deposit over the cathode while recovering the impurity-free HCl. These electrodepositions have been performed in galvanostatic mode at two current densities: — 50 and —100 mA·cm^2, corresponding to the reduction waves R1 and R2 observed in **Fig. 4**.

3.3.1. Results obtained with the three-compartment reactor

The three-compartment reactor configuration (**Fig. 1**) allows chloride ions to pass from the cathodic compartment to the central one through the anion-exchange membrane. The role of the cation-exchange membrane is to prevent that chloride ions could reach the anodic compartment, thus avoiding its oxidation to chlorine gas at the anode. Moreover, the H^+ ions generated at the anode can also migrate towards the central compartment, thus contributing to increase the concentration of the recovered HCl. In this manner, elements from the real effluent, such as antimony and bismuth, can be recovered at the cathode; and impurity-free HCl would be concentrated in the central compartment for its direct reuse in the industrial process.

Fig. S.1 of the supplementary material shows the evolution of the chloride ion concentration in the cathodic and central compartments for the electrodeposition test carried out at an applied current density of —100 mA-cm^{-2}. During the first 60 min, the chloride concentration in the cathodic compartment decreases, while it increases in the central one, as expected. However, after 60 min, the flux of Cl^- ions towards the central compartment decreases notably. An explanation for this behavior could be an increase in the transport rate of protons through the anion-exchange membrane, thus hindering the passage of chloride ions. At high concentration levels, as is the case (5.6 M HCl), protons can pass through the anion-exchange membrane towards the cathodic compartment due to their smaller size and higher mobility, compared to other ions. At the end of the experiment, the concentration of Cl^- ions in the central compartment was 1.7 M, a value quite far from the HCl concentration in the real effluent under study. Regarding the anodic compartment, analysis of the final samples confirmed that Cl^- ions do not reach the anodic compartment, thus, they are efficiently rejected by the cation-exchange membrane.

According to the results obtained, we can conclude that it is not possible to reach concentration levels similar to those of the eluent used to regenerate the resins ($[HCl] \sim 5.6$ M) in the central compartment with the configuration studied. Two possible changes to improve the process could be the use of anion-exchange membranes with specific properties to block the passage of protons [**43,44**] or using a cell configuration with multiple membrane pairs that could achieve the desired increase in HCl concentration.

Fig. 7 represents the evolution of the relative concentrations of antimony, bismuth, arsenic and copper in the cathodic compartment at the two applied current densities. In general, an increase in the applied current density from — 50 to —100 mA·cm^{-2} implies a higher recovery percentage for the four elements. Regarding antimony (**Fig. 7**a), this element was depleted in the effluent at the end of the test when a current density of —100 mA-cm^{-2} was applied; however, at a current density of —50 mA·cm^{-2}, only 60 % of the antimony present in the solution was deposited at the cathode. **Fig. 7**b shows that the electrodeposition of bismuth does not present such a strong dependence on the applied current density as that observed for antimony; this behavior was also detected in a previous work [**38**]. Practically 95 % of bismuth was deposited when applying —100 mA·cm^{-2}, and this percentage decreased to approximately 80 % at — 50 mA·cm^{-2}. In the case of arsenic (**Fig. 7**c), it was not possible to recover more than 70 % during the 4 h of the test for the highest applied current density; therefore, it would be necessary to perform longer deposition tests to achieve full recovery of arsenic. The lower recovery rate of arsenic may be related to the low current density observed in the associated reduction peak (C0, **Fig. 3**b), which reflects its slower deposition compared to that of antimony and bismuth. Finally, **Fig. 7**d shows that practically 90 % of copper was deposited when applying —100 mA·cm^{-2}, but at — 50 mA·cm^{-2} this percentage decreases to 40 %. This could be attributed to the fact that, by applying the lowest current density, the reduction wave R2 observed for copper in **Fig. 4** has not been reached yet. At the end of the test conducted at —100 mA·cm^{-2}, the recovered moles of antimony

represent approximately 78 % of the total recovered moles of all metals. Although almost all bismuth contained in the solution is deposited, this element only represents 5 % of the total moles deposited; arsenic, 11 %; and copper, 6 %. Consequently, the deposits obtained would have a high content in antimony, which is consistent with the composition of the deposits obtained in potentiostatic mode.

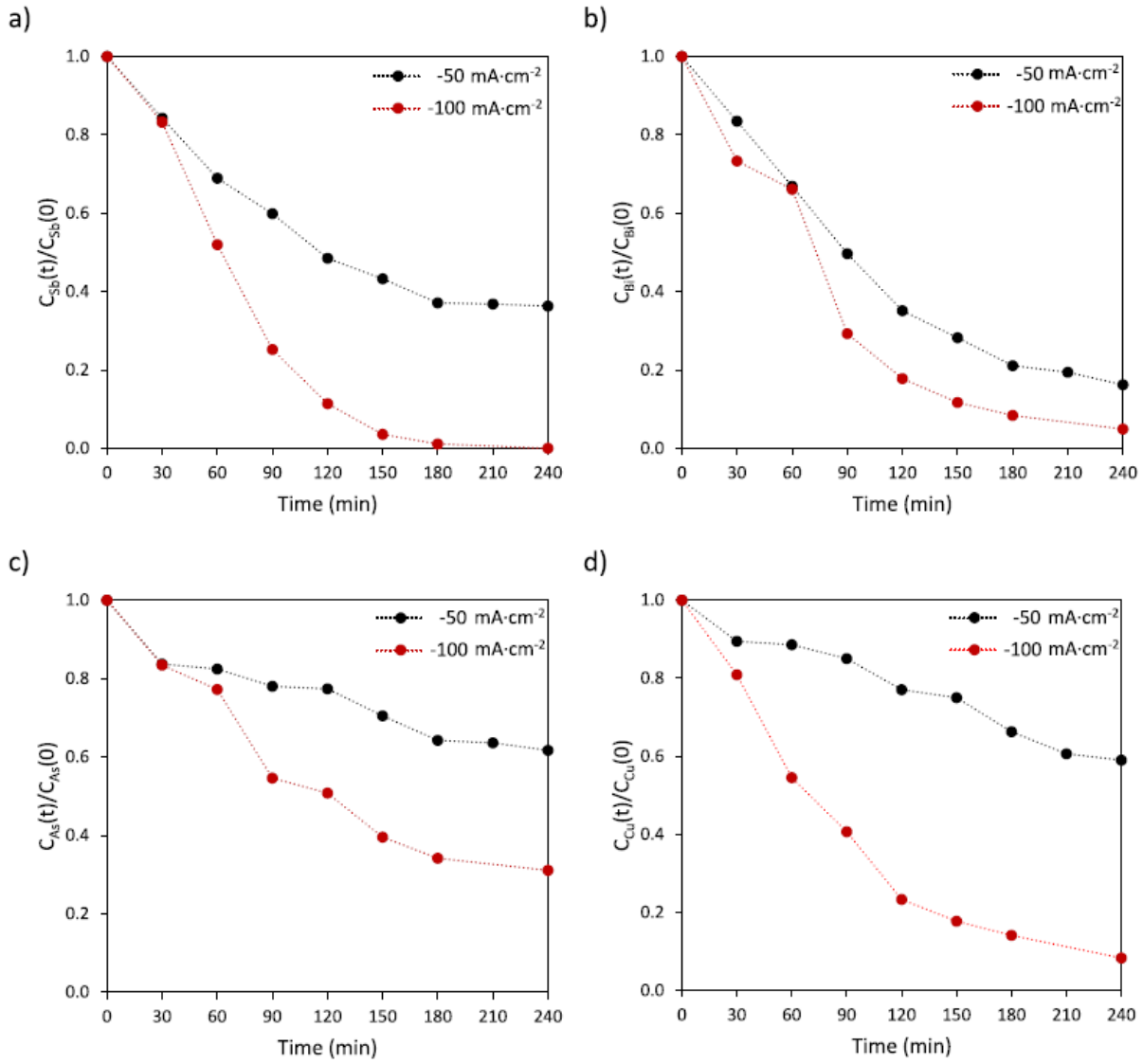

Fig. 7. Evolution over time of the relative concentration of antimony (a), bismuth (b), arsenic (c), and copper (d) in the cathodic compartment of the three-compartment reactor at two applied current densities, — 50 and —100 mA·cm^{-2}.

Therefore, it has been proven that the main elements present in the real effluent can be recovered at the cathode, achieving a complete recovery of antimony working at —100 mA·cm^{-2} after 4 h. Although it is not possible to reach very high HCl concentrations in the central compartment of the cell, impurity-free HCl could be obtained in the cathodic compartment with a final concentration of 4.8 M (**Fig. S.1**).

3.3.2. Comparison with the single-compartment reactor

Electrodeposition of antimony in a highly concentrated hydrochloric acid solution can be affected by the occurrence of two secondary reactions: the evolution of hydrogen and the generation of chlorine

gas [**34**]. HER generates bubbles at the cathode surface that can decrease its effective area and also diminishes the efficiency of the electrodeposition process because both are competing reduction reactions. Regarding the generation of chlorine at the anode, it is a highly oxidizing chemical that can cause the redissolution of the deposits [**45**]. The objective of performing tests in a single-compartment reactor is to evaluate the effect of these secondary reactions on the electrodeposition of elements present in the effluent. A current density of —100 mA·cm^{-2} has been applied because this is the value that has shown the best results when using the three-compartment reactor.

Fig. 8 compares the evolution of the relative concentrations of antimony, bismuth, arsenic and copper between the single- and three-compartment reactors. In general, the use of the single-compartment reactor leads to a slower electrodeposition of the four elements. In our previous research conducted with a synthetic solution of antimony and bismuth in 6 M HCl [**38**], it was concluded that with the highest concentration of Sb in the solution (10 mM Sb and nSb/nBi equal to 4) and at the highest applied current density (—4.5 mA·cm^{-2}), the main reaction that takes place during electrodeposition is the HER. The real effluent used in the present work has a much higher concentration of Sb compared to the previous study (188.81 mM Sb and nSb/nBi equal to 15), so that higher current densities (—100 mA-cm^{-2}) are necessary to electrodeposit the metals in a reasonable time. Therefore, with this effluent, the influence of the HER is expected to be greater. Additionally, in another previous work [**34**] with a synthetic solution of antimony 2 mM in 6 M HCl, it was found that the redissolution of the Sb deposits due to the chlorine generated was relevant only at the highest current density applied (—2.5 mA·cm^{-2}). In the present work, by using the real effluent, which has a significantly higher concentration of Sb, and applying higher current densities, the problems due to the chlorine produced are expected to be greater. Results presented in **Fig. 8** corroborate that the chlorine gas generated influences negatively the electrodeposition of the elements. Furthermore, the difference between using a single-compartment reactor and a membrane reactor is very notorious with the real effluent due to the high applied current densities (—100 mA·cm^{-2}). This means that, with the real effluent, the advantages of using electromembrane reactors are greater. In this case, using electrochemical reactors with separated compartments is crucial to avoid the formation of chlorine gas at the anode and the subsequent redissolution of the deposited metals.

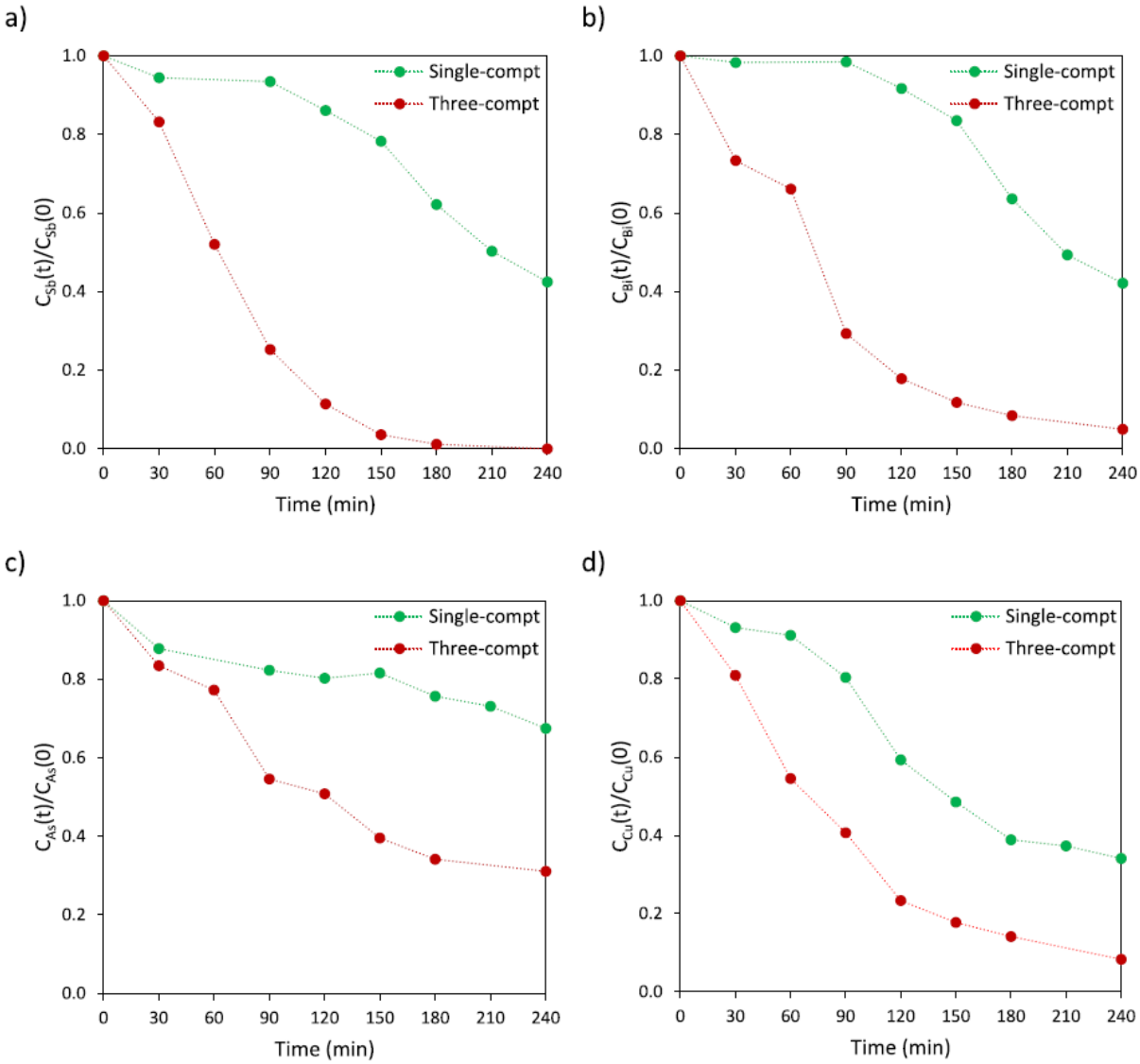

Fig. 8. Comparison of the evolution over time of the relative concentration of antimony (a), bismuth (b), arsenic (c) and copper (d) between the single- and three-compartment reactors at an applied current density of —100 mA·cm^{-2}.

3.3.3. Analysis of the current efficiency and specific energy consumption

The current efficiency (ϕ) for the deposition of each element has been calculated according to the following equation:

$$\phi(t) = \frac{n \cdot F \cdot V \cdot (C(0) - C(t))}{\int_0^t I(t)dt} \cdot 100(\%) \qquad (2)$$

where n is the number of electrons exchanged (for antimony, bismuth and arsenic n is equal to 3; and for copper n is equal to 2); F is Fadaray's constant (96,485.33C-mol^{-1}); V is the electrochemical reactor volume (L); $C(0)$ and $C(t)$ are the concentration of the elements (mol-L^{-1}) in the effluent and that measured at a given time t, and $I(t)$ is the function of applied current over time (A). **Fig. 9** shows the total current efficiency, calculated as the sum of the current efficiencies for the four elements ($\phi_{Sb} + \phi_{Bi} + \phi_{As} + \phi_{Cu}$), and the current efficiencies for each of the elements.

Regarding the total current efficiency (**Fig. 9**a), the highest values were obtained in the test carried out at — 50 mA·cm^{-2} with the three-compartment reactor; however, current efficiency decreases fast with time. These values are higher than those obtained at —100 mA·cm^{-2} with the same reactor, even though a higher percentage of the four elements was deposited at the highest current (**Fig. 7**). This result can be attributed to the contribution of secondary reactions, which becomes more relevant at increasing current densities. At —100 mA·cm^{-2}, a large portion of the applied current density is not used in the reduction of the elements but in the HER, thus decreasing the value of efficiency. At — 100 mA·cm^{-2}, with both reactors, a moderate decrease in efficiency is observed over time, because HER is already significant from the beginning of the tests. With the single-compartment reactor, the efficiency values reach stable values around 15 %.

The behavior of the current efficiency for each of the elements (**Fig. 9**) is analogous to that observed for the total current efficiency, that is, the highest values were obtained in the tests carried out with the three-compartment reactor and, in particular, at — 50 mA·cm^{-2}. For antimony (**Fig. 9**b), the current efficiency decreases over time when using the three-compartment reactor; however, this parameter remains between 3 and 9 % with the single-compartment reactor. The current efficiency for bismuth (**Fig. 9**c) shows a practically constant value over time. Furthermore, current efficiency for bismuth deposition is much lower than for antimony and arsenic because the concentration of bismuth in the real effluent under study is significantly lower, especially when compared to antimony (12.61 mM Bi and 188.81 mM Sb). The current efficiency obtained for arsenic (**Fig. 9**d) shows its maximum value at the beginning of the process and then decreases and remains almost stable during the final 2 h. Additionally, the values for arsenic are lower than those for antimony, since the concentration of arsenic (40.20 mM) in the effluent is lower. Regarding copper (**Fig. 9**e), the current efficiency values are very similar to those for bismuth because the copper concentration (16.46 mM) in the real effluent is of the same order of magnitude; and they also show a practically constant value over time.

The specific energy consumption (Es) has been calculated for the main element recovered (i.e. antimony) according to the following equation:

$$E_s(t) = \frac{\int_0^t U(t)\cdot I(t)dt}{M\cdot V\cdot (C(0)-C(t))\cdot 3600}(kW\cdot h\cdot kg^{-1}) \qquad (3)$$

where $C(0)$ and $C(t)$ are the concentration of antimony in the solution (mol· L^{-1}) at the beginning of the tests and at a specific time, respectively; V is the reactor volume (L); $I(t)$ is the function of applied current with time (A); M corresponds to the element atomic weight (121.76 g·mo^{-1}); and $U(t)$ is the cell voltage as a function of time (V).

Fig. S2a of the Supplementary material shows the evolution over time of specific energy consumption for antimony. As could be expected, the highest values were obtained in the test carried out at —100 mA-cm^{-2} with the three-compartment reactor since both the applied current and the cell voltage drop are the highest. At the end of the experiment, when all antimony has been completely recovered, the specific energy consumption for antimony is 72 kWh·kg^{-1}. If the other recovered metals (i.e. bismuth, arsenic and copper) are also considered, the specific energy consumption at the end of the experiment is 31 kWh·kg^{-1} (see **Fig. S2b of the Supplementary material**). Results obtained with the single-compartment reactor and at lower current density exhibit a decrease of the specific energy consumption; however, these conditions do not lead to the complete removal of antimony. Garrido et al. [**46**] have recently investigated the recovery of Sb from a solution with a composition similar to the real effluent analyzed in this work (6 M of HCl, 20 g· L^{-1} of Sb and 4 g· L^{-1} of Bi). These authors employed a two-compartment reactor where a cation-exchange membrane was used as a separator, obtaining a specific energy consumption per kg of recovered Sb equal to 1.76 kWh·kg^{-1} without

depleting it from the solution. It can be noted that the reactor configuration is not the same, but the convenience of using electromembrane reactors is confirmed. In terms of energy consumption, and given the fact that pure HCl can be better recovered in the cathodic compartment, a two-compartment configuration would be the most efficient configuration, because the cell voltage drop could be reduced by decreasing the distance between anode and cathode, as compared with the three-compartment reactor.

4. Conclusions

In this work, electrodeposition has been proposed to regenerate spent eluates of ion-exchange resins utilized in the copper electrorefining process and recover critical raw materials present in it. Four reduction peaks were detected at + 0.30, —0.20, —0.34 and — 0.50 $V_{Ag/AgCl}$ during the electrochemical characterization of a real effluent. The first peak is related to the reduction of Cu(II) to Cu(I); the second, to the reduction of As(III) to metallic As; the third is mainly associated with the deposition of Sb and Bi as an alloy; and, the fourth, with the reduction of Cu(I) to metallic Cu. The linear voltammogram registered presents three reduction waves analogous to the reduction peaks detected in the cyclic voltammograms.

Short-term electrodepositions were carried out in potentiostatic mode at the three potentials corresponding to the observed waves. The composition of the deposits confirms that the reduction of arsenic, antimony and bismuth, and copper take place at the studied potentials, whereas the reduction of the rest of the elements (Fe, Ni, Zn, Cd, Pb) present in the effluent does not occur in significant proportions. In addition, the electrodeposition process shows a great selectivity towards antimony over arsenic, and even over copper at the least cathodic potentials, but not over bismuth. Selectivity towards antimony decreases when more negative potentials are applied. Thus, it would be possible to obtain a deposit with a high content in antimony (85 wt%) working at the least cathodic potential studied, — 0.25 $V_{Ag/AgCl}$.

The results obtained in long-term galvanostatic electrodeposition tests, using the three-compartment reactor demonstrated that it is not possible to concentrate hydrochloric acid (HCl) in a separate compartment up to the initial eluent concentration with this configuration. However, it is possible to recover the main elements present in the real effluent through their electrodeposition at the cathode; this allowing to obtain impurity-free HCl in the cathodic compartment. A complete recovery of antimony and almost complete recovery of bismuth and copper were achieved working at —100 mA·cm^{-2} after 4 h of test, but it would be necessary to extend the duration of the electrodeposition tests to achieve the total recovery of arsenic. Another option would be to apply lower current densities, but increasing the duration of the tests even further, to improve the efficiency of the process.

Finally, the long-term electrodeposition test conducted with the single-compartment reactor has revealed the need to use membrane reactors in order to prevent the formation of chlorine gas, which attacks the metallic deposits. In general, the use of an electromembrane reactor results in higher current efficiencies.

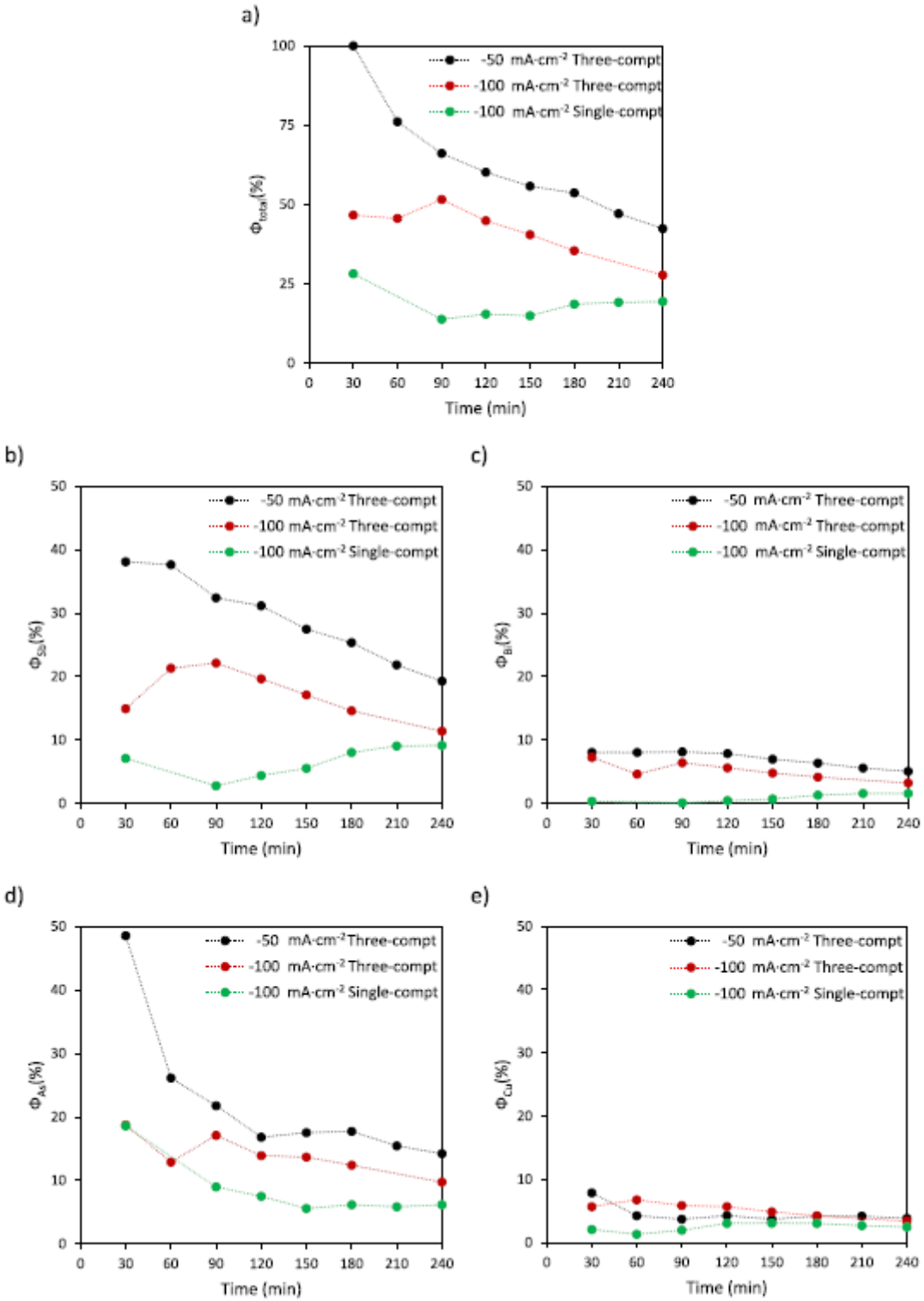

Fig. 9. Evolution over time of the total current efficiency (a) and the current efficiency for antimony (b), bismuth (c), arsenic (d) and copper (e) at two applied current densities, — 50 and —100 mA·cm^{-2}, using the three-compartment reactor, and at —100 mA·cm^{-2} using the single-compartment reactor.

References

[1] European Commission, Study on the critical raw materials for the EU 2023 - Final report, Publications Office of the European Union, 2023. Doi: doi/10.2873/725585.

[2] U.S. Geological Survey, 2022 Final List of Critical Minerals, Fed Regist 87 (2022) 10381-10382.

[3] U.S. Geological Survey, Mineral Commodity Summaries, 2023. Doi: 10.3133/ mcs2023.

[4] H. Ling, A. Malfliet, B. Blanpain, M. Guo, A review of the technologies for antimony recovery from refractory ores and metallurgical residues, Miner. Process. Extr. Metall. Rev. (2022), **https://doi.org/10.1080/08827508.2022.2132946**.

[5] M.L.C.M. Henckens, P.P.J. Driessen, E. Worrell, How can we adapt to geological scarcity of antimony? Investigation of Antimony's Substitutability and of Other Measures to Achieve a Sustainable Use, Resour Conserv Recycl 108 (2016) 54-62, **https://doi.org/10.1016Zj.resconrec.2016.01.012**.

[6] S. Carrara, S. Bobba, D. Blagoeva, P. Alves Dias, A. Cavalli, K. Georgitzikis, M. Grohol, A. Itul, T. Kuzov, C. Latunussa, L. Lyons, G. Malano, T. Maury, A. Prior Arce, J. Somers, T. Telsnig, C. Veeh, D. Wittmer, C. Black, D. Pennington, M. Christou, Supply chain analysis and material demand forecast in strategic technologies and sectors in the EU - A foresight study, Luxembourg Doi: 10.2760/ 334074 (2023) JRC132889.

[7] M. Moats, L. Alagha, K. Awuah-Offei, Towards resilient and sustainable supply of critical elements from the copper supply chain: A review, J Clean Prod 307 (2021) 127207, **https://doi.org/10.1016/JJCLEPRO.2021.127207**.

[8] A.J. Rosario-Beltré, J. Sánchez-España, V. Rodríguez-Gómez, F.J. Fernández-Naranjo, E. Bellido-Martín, P. Adánez-Sanjuán, J.C. Arranz-González, Critical Raw Materials recovery potential from Spanish mine wastes: A national-scale preliminary assessment, J Clean Prod 407 (2023) 137163, **https://doi.org/ 10.1016/j.jclepro.2023.137163**.

[9] D. Dupont, S. Arnout, P.T. Jones, K. Binnemans, Antimony recovery from end-of-life products and industrial process residues: a critical review, Journal of Sustainable Metallurgy 2 (2016) 79-103, **https://doi.org/10.1007/s40831-016-0043-y**.

[10] S.A. Awe, K. Sandström, Selective leaching of arsenic and antimony from a tetrahedrite rich complex sulphide concentrate using alkaline sulphide solution, Miner Eng 23 (2010) 1227-1236, **https://doi.org/10.1016/j.mineng.2010.08.018**.

[11] R.R. Moskalyk, A.M. Alfantazi, Review of copper pyrometallurgical practice: today and tomorrow, Miner Eng 16 (2003) 893-919, **https://doi.org/10.1016/j. mineng.2003.08.002**.

[12] P. Navarro, J. Simpson, F.J. Alguacil, Removal of antimony (III) from copper in sulphuric acid solutions by solvent extraction with LIX 1104SM, Hydrometall. 53 (1999) 121-131, **https://doi.org/10.1016/S0304-386X(99)00033-X**.

[13] X. Wang, X. Wang, B. Liu, M. Wang, H. Wang, X. Liu, S. Zhou, Promotion of copper electrolyte self-purification with antimonic oxides, Hydrometall. 175 (2018) 28-34, **https://doi.org/10.1016/j.hydromet.2017.10.028**.

[14] S. Jafari, M. Kiviluoma, T. Kalliomaki, E. Klindtworth, A.T. Aji, J. Aromaa, B. P. Wilson, M. Lundstrom, Effect of typical impurities for the formation of floating slimes in copper electrorefining, Int J Miner Process 168 (2017) 109-115, **https:// doi.org/10.1016/j.minpro.2017.09.016**.

[15] P. Navarro, F.J. Alguacil, Adsorption of antimony and arsenic from a copper electrorefining solution onto activated carbon, Hydrometall. 66 (2002) 101-105, **https://doi.org/10.1016/S0304-386X(02)00108-1**.

[16] K.S. Barros, V.S. Vielmo, B.G. Moreno, G. Riveros, G. Cifuentes, A.M. Bernardes, Chemical composition data of the main stages of copper production from sulfide minerals in Chile: a review to assist circular economy studies, Minerals 12 (2022), **https://doi.org/10.3390/min12020250**.

[17] F. Arroyo-Torralvo, A. Rodríguez-Almansa, I. Ruiz, I. González, G. Ríos, C. Fernaóndez-Pereira, L.F. Vilches-Arenas, Optimizing operating conditions in an ion-exchange column treatment applied to the removal of Sb and Bi impurities from an electrolyte of a copper electrorefining plant, Hydrometall. 171 (2017) 285-297, **https://doi.org/10.1016/j.hydromet.2017.06.009**.

[18] T. Nagai, Purification of copper electrolyte by solvent extraction and ion-exchange techniques, Miner. Process. Extr. Metall. Rev. 17 (1997) 143-168, **https://doi.org/ 10.1080/08827509708914145**.

[19] G. Cifuentes, M. Agurto, S. Di, I. Gentico, M. Cifuentes-Cabezas, Antimony Recovery by Electro-Electrodialysis (EED) (2019), **https://doi.org/10.19080/ IJESNR.2022.31.556310**.

[20] N. Benabdallah, D. Luo, M. Hadj Youcef, J. Lopez, M. Fernández de Labastida, A. M. Sastre, C.A. Valderrama, J.L. Cortina, Increasing the circularity of the copper metallurgical industry: Recovery of Sb(III) and Bi(III) from hydrochloric solutions by integration of solvating organophosphorous extractants and selective precipitation, Chemical Engineering Journal 453 (2023) 10-14, **https://doi.org/ 10.1016/j.cej.2022.139811**.

[21] A. Artzer, M. Moats, J. Bender, Removal of antimony and bismuth from copper electrorefining electrolyte: Part I—A review, JOM 70 (2018) 2033-2040, **https:// doi.org/10.1007/s11837-018-3075-x**.

[22] K.C. Sole, M.B. Mooiman, E. Hardwick, Ion exchange in hydrometallurgical processing: An overview and selected applications, Sep. Purif. Rev. 47 (2018) 159-178, **https://doi.org/10.1080/15422119.2017.1354304**.

[23] E. Diaz Gutiérrez, J.A. Maldonado Calvo, J.M. Gallardo Fuentes, A. Paul Escolano, Effect of pH hydrolysis on the recovery of antimony from spent electrolytes from copper production, Materials 16 (2023) 1-12, **https://doi.org/10.3390/ ma16113918**.

[24] Y. Yang, C. Lan, Y. Wang, Z. Zhao, B. Li, Recycling of ultrafine NdFeB waste by the selective precipitation of rare earth and the electrodeposition of iron in hydrofluoric acid, Sep Purif Technol 230 (2020), **https://doi.org/10.1016/j. seppur.2019.115870**.

[25] W. Jin, Y. Zhang, Sustainable electrochemical extraction of metal resources from waste streams: from removal to recovery, ACS Sustain Chem Eng (2020), **https:// doi.org/10.1021/acssuschemeng.9b07007**.

[26] R.D. Armstrong, M. Todd, J.W. Atkinson, K. Scott, Selective electrodeposition of metals from simulated waste solutions, J Appl Electrochem 26 (1996) 379-384, **https://doi.org/10.1007/BF00251322**.

[27] M. García-Gabaldón, V. Pérez-Herranz, J. García-Antón, J.L. Guinón, Electrochemical recovery of tin and palladium from the activating solutions of the electroless plating of polymers

Potentiostatic operation, Sep Purif Technol 45 (2005) 183-191, **https://doi.org/10.1016/j.seppur.2005.03.008**.

[28] V.R.C. Thanu, M. Jayakumar, Electrochemical recovery of antimony and bismuth from spent electrolytes, Sep Purif Technol 235 (2020) 116169, **https://doi.org/ 10.1016/j.seppur.2019.116169**.

[29] Y. Liu, Y.Y. Deng, Q. Zhang, H. Liu, Overview of recent developments of resource recovery from wastewater via electrochemistry-based technologies, Sci. Total Environ. 757 (2021) 143901, **https://doi.org/10.1016/J. SCITOTENV.2020.143901**.

[30] L. Yang, W. Hu, Z. Chang, T. Liu, D. Fang, P. Shao, H. Shi, X. Luo, Electrochemical recovery and high value-added reutilization of heavy metal ions from wastewater: Recent advances and future trends, Environ Int 152 (2021) 106512, **https://doi. org/10.1016/J.ENVINT.2021.106512**.

[31] J. Carrillo-Abad, M. Garcia-Gabaldon, I. Ortiz-Gandara, E. Bringas, A.M. Urtiaga, I. Ortiz, V. Perez-Herranz, Selective recovery of zinc from spent pickling baths by the combination of membrane-based solvent extraction and electrowinning technologies, Sep Purif Technol 151 (2015) 232-242, **https://doi.org/10.1016/j. seppur.2015.07.051**.

32] G. Stando, P.M. Hannula, B. Kumanek, M. Lundström, D. Janas, Copper recovery from industrial wastewater - Synergistic electrodeposition onto nanocarbon materials, Water Resour Ind 26 (2021), **https://doi.org/10.1016/j. wri.2021.100156**.

[33] L. Hernández-Pérez, J. Carrillo-Abad, E.M. Ortega, V. Pérez-Herranz, M. T. Montañés, M.C. Marti-Calatayud, Voltammetric and electrodeposition study for the recovery of antimony from effluents generated in the copper electrorefining process, J. Environ. Chem. Eng. 11 (2023) 109139, **https://doi.org/10.1016/jjece: 2022.109139**.

[34] L. Hernández-Pérez, J. Carrillo-Abad, V. Pérez-Herranz, M.T. Montañés, M. C. Marti-Calatayud, Effluents from the copper electrorefining as a secondary source of antimony: Role of mass transfer on the recovery by electrodeposition, Desalination 549 (2023) 116322, **https://doi.org/10.1016/j.desal.2022.116322**.

[35] D. Luo, M. Fernández de Labastida, J.L. Cortina, J. Lopez, Recovery of antimony and bismuth from arsenic-containing waste streams from the copper electrorefining circuit: An example of promoting critical metals circularity from secondary resources, J Clean Prod 415 (2023) 137902, **https://doi.org/10.1016/). jclepro.2023.137902**.

[36] E. Díaz, J.A. Maldonado Calvo, J.M. Gallardo, A. Paul, Extraction of antimony from a hydrochloric acid side stream of copper electrorefining by hydrolysis, Hydrometallurgy 219 (2023), **https://doi.org/10.1016/j.hydromet.2023.106076**.

[37] Q. Tian, G. Li, Y. Xin, X. Lv, X. Lv, W. Yu, K. Yan, Comprehensive treatment of acid effluent containing antimony and arsenic by selective reduction and evaporative crystallization, Hydrometall. 195 (2020) 105366, **https://doi.org/10.1016/). hydromet.2020.105366**.

[38] L. Hernández-Pérez, A. Muñoz-Pérez, E.M. Ortega, V. Pérez-Herranz, M. T. Montañés, M.C. Marti-Calatayud, Increasing the sustainability of copper electrorefining: Selective electrodeposition of antimony in the presence of bismuth from highly concentrated hydrochloric acid effluents, J. Environ. Chem. Eng. 12 (2024) 112005, **https://doi.org/10.1016/j.jece:2024.112005**.

[39] P.A. Riveros, J.E. Dutrizac, R. Lastra, A study of the ion exchange removal of antimony(III) and antimony(V) from copper electrolytes, Can. Metall. Q. 47 (2008) 307-316, **https://doi.org/10.1179/cmq.2008.47.3.307**.

[40] F. Besse, C. Boulanger, J.M. Lecuire, Preparation of Bi^Sbx films by electrodeposition, J Appl Electrochem 30 (2000) 385-392, **https://doi.org/ 10.1023/A:1003990327662**.

[41] Y. Xiang Shu, H. Zhen Cao, H. Bin Zhang, S. Hang Xu, G. Ya Hou, Y. Ping Tang, G. Qu Zheng, Composition and structure of arsenic-antimony alloy electrodeposited from acidic chloride solution, Transactions of Nonferrous Metals Society of China 31 (2021) 2861-2870. Doi: 10.1016/S1003-6326(21)65699-6.

[42] L.K. Wu, Y.Y. Li, H.Z. Cao, G.Q. Zheng, Copper-promoted cementation of antimony in hydrochloric acid system: A green protocol, J Hazard Mater 299 (2015) 520-528, **https://doi.org/10.1016/j.jhazmat.2015.07.053**.

[43] S. Yu, H. Qian, J. Liao, J. Dong, L. Yu, C. Liu, J. Shen, Proton blockage PVDF-co-HFP-based anion exchange membrane for sulfuric acid recovery in electrodialysis, J Memb Sci 653 (2022), **https://doi.org/10.1016/j.memsci.2022.120510**.

[44] L. Wang, Z. Li, Z. Xu, F. Zhang, J.E. Efome, N. Li, Proton blockage membrane with tertiary amine groups for concentration of sulfonic acid in electrodialysis, J Memb Sci 555 (2018) 78-87, **https://doi.org/10.1016/j.memsci.2018.03.011**.

[45] E. Kim, M. Kim, J. Lee, J. Jeong, B.D. Pandey, Leaching kinetics of copper from waste printed circuit boards by electro-generated chlorine in HCl solution, Hydrometall. 107 (2011) 124-132, **https://doi.org/10.1016/). hydromet.2011.02.009**.

[46] B. Garrido, J. Lara, J. Moreno, A. Giacobbo, E. Pino, G. Cifuentes, A.M. Bernardes, Antimony recovery from copper refining electrolyte by membrane electrolysis, REM-International Engineering Journal 78 (2025) e240031.